





Repurposed Nrf2 activator dimethyl fumarate rescues muscle inflammation and fibrosis in an aggravated *mdx* mouse model of Duchenne muscular dystrophy

Stephanie Kourakis^{a,b,1} , Cara A. Timpani^{a,b,c,1}, Ryan M. Bagaric^{a,b}, Bo Qi^{a,b}, Benazir A. Ali^{a,b}, Rebecca Boyer^a, Guinevere Spiesberger^{a,b}, Nitika Kandhari^d, Xu Yan^{a,e}, Jujiao Kuang^a, Ankita Tulangekar^{a,b}, Judy B. de Haan^{f,g}, Deanna Deveson-Lucas^d, Nicole Stupka^{c,a}, Dirk Fischer^h, Emma Rybalka^{a,b,*} 

^a Institute for Health and Sport (IHes), Victoria University, Melbourne, Victoria, Australia

^b Inherited and Acquired Myopathies Program, Australian Institute for Musculoskeletal Science (AIMSS), St Albans, Victoria, Australia

^c Department of Medicine – Western Health, Melbourne Medical School, The University of Melbourne, St Albans, Victoria, Australia

^d Monash Genomics and Bioinformatics Platform, Biomedical Discovery Institute, Monash University, Clayton, Victoria, Australia

^e Sarcopenia Research Program, Australian Institute for Musculoskeletal Science (AIMSS), St Albans, Victoria, Australia

^f Basic Science Domain, Oxidative Stress Laboratory, Baker Heart and Diabetes Institute, Melbourne, Victoria, Australia

^g Baker Department of Cardiometabolic Health, University of Melbourne, Parkville, Victoria, Australia

^h Division of Neuropediatric and Developmental Medicine, University Children's Hospital of Basel (UKBB), Basel, Switzerland

ARTICLE INFO

Keywords:

Duchenne muscular dystrophy
Dimethyl fumarate
Therapeutics
Muscle pathology

ABSTRACT

In inherited neuromuscular disease, Duchenne muscular dystrophy (DMD), glucocorticoids significantly slow disease progression yet impart side effects severe enough to preclude use in a significant proportion of patients. Extending our findings that acute treatment with FDA approved multiple sclerosis drug, dimethyl fumarate (DMF), rescues muscle pathology in juvenile *mdx* mice, we aimed to conduct tiered pre-clinical testing toward translation. To aggravate disease phenotype in adult *mdx* muscles that usually lack human equivalent muscle pathology, we used bi-weekly treadmill running for 4 weeks which increased plasma DMD biomarker, creatine kinase, by 2-fold and quadriceps fibrosis by ~30%. Using this model, we screened DMF for 5 weeks in a head-to-head comparison, and in combination, with standard-of-care prednisone (PRED), to model the most likely clinical trial scenario. We show comparable efficacy between DMF and PRED at reducing inflammation via NF- κ B suppression and CD68⁺ macrophage infiltration. Moderate term DMF monotherapy had additional anti-fibrotic and anti-lipogenic effects on skeletal and cardiac muscle beyond those seen with PRED treatment, although combination therapy exacerbated fibrosis in quadriceps. Our study supports DMF as a repurposing candidate for DMD, especially for patients who cannot tolerate chronic glucocorticoid treatment. We also highlight the importance of evaluating combination therapy to identify potential off-target effects between emerging therapeutics and glucocorticoids towards better designed clinical trials.

1. Introduction

Duchenne muscular dystrophy (DMD) is a severe, progressive, muscle-wasting disease caused by mutations in the *DMD* gene. Dystrophin loss disrupts the junction between the intracellular cytoskeleton and extracellular matrix (ECM), which stabilises muscle fibres during contraction. Dystrophin deficiency results in chronic muscle damage,

degradation, fibrosis and replacement of skeletal muscle with fatty infiltrates [1]. Affecting predominantly males, DMD is typically diagnosed by ~5 years of age presenting as delayed motor milestones and frequent falls and by early adolescence, loss of ambulation and pulmonary function decline is common [2,3]. Pulmonary distress is complicated by diaphragmatic weakness and fibrosis, and scoliosis, which alters the shape of the thoracic cavity and reduces respiratory capacity [4].

* Corresponding author. Institute for Health and Sport (IHes), Victoria University, Melbourne, Victoria, Australia.

E-mail address: emma.rybalka@vu.edu.au (E. Rybalka).

¹ Co-first authors.

Natural history data suggest that cardiac symptoms emerge from as early as 12–14 years leading to dilated cardiomyopathy in almost all patients, even with prophylactic treatment with cardiac medications, which can delay the onset.

The DMD therapeutic landscape has expanded significantly over the past decade. Since 2016, four exon-skipping antisense oligonucleotide drugs (Exondys 51, Vyondys 53, Viltepso and Amondys 45) and two gene replacement therapies (Elevidys and fordadistrogene movaparvovec) have been granted accelerated access [5]. However, their efficacy is unclear, and fatalities have occurred with gene replacement strategies raising safety concerns [6]. While these therapies may have the best potential of providing long-term disease-modifying benefits to amenable patients, there are relatively fewer therapeutics in development to

address the secondary pathomechanisms, especially the hyper-inflammation and chronic immune system activation that drives muscle fibrosis, weakness and loss of function [7]. Targeting this aspect, anti-inflammatory corticosteroids have prevailed as pharmacological standard of care (SOC) for DMD for more than three decades. With early intervention, they effectively slow disease progression, prolonging ambulation, and pulmonary function. Yet they have an extensive side-effect profile, e.g., weight gain, osteoporosis, adrenal insufficiency, metabolic syndrome and behavioural issues [8], which limits their clinical utility in as many as 37 % of patients [9]. Approved in 2023, steroid analogue Agamree (vamorolone) was developed to reduce the side-effect profile but retain full immunomodulatory and anti-inflammatory function. However, some corticosteroid side effects

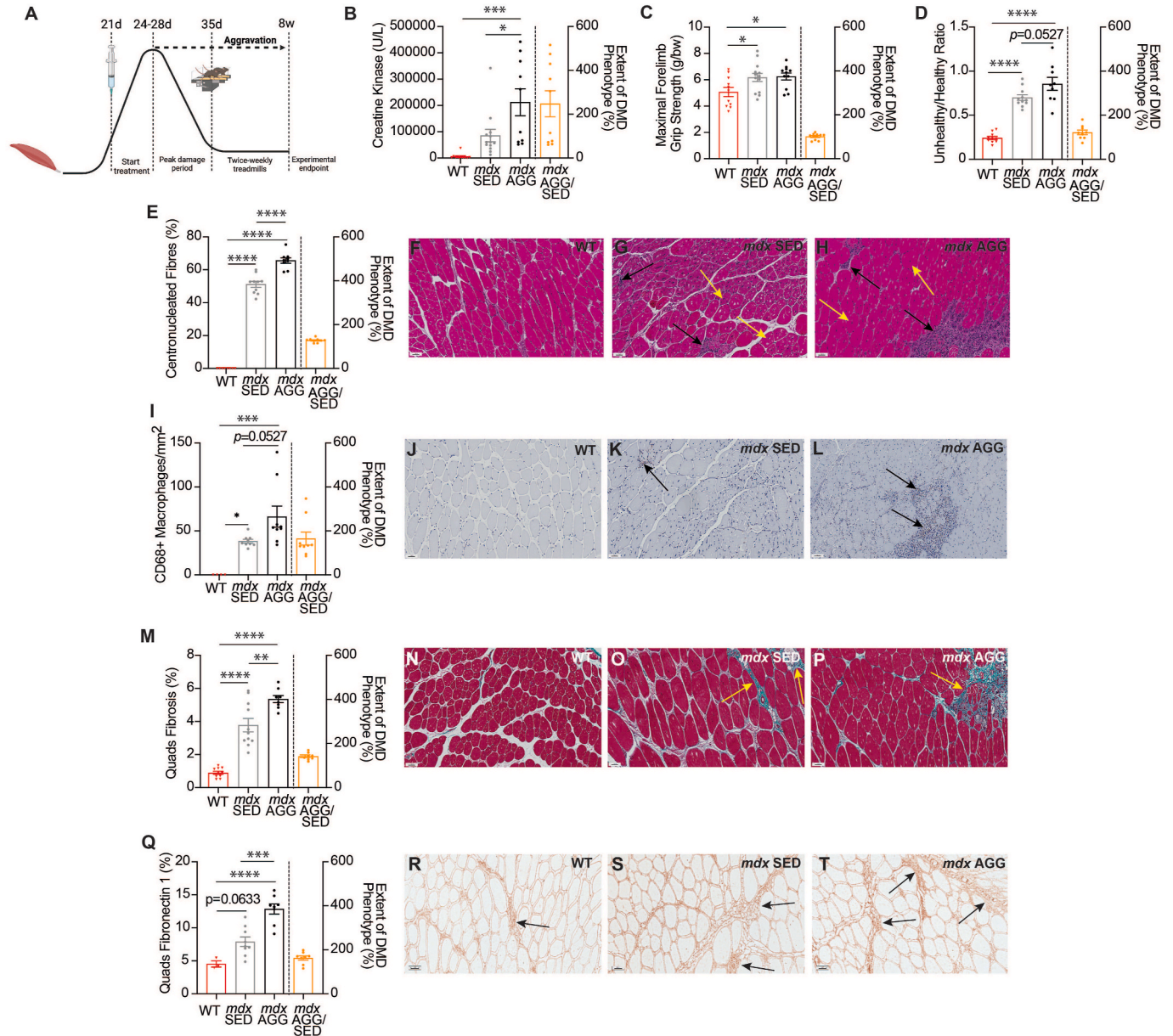


Fig. 1. Twice-weekly forced treadmill running aggravates the *mdx* phenotype. (A) Schematic of treatment and treadmill protocols. *Mdx* aggravation was proved using clinically compatible parameters of (B) plasma creatine kinase and (C) forelimb grip strength. H&E staining assessed the (D) unhealthy/healthy tissue ratio (black arrows) and (E) centronucleated fibre proportion (orange arrows) of the quadriceps (F–H). Pan macrophage marker, CD68, and Masson's trichrome staining assessed (I–L) immune infiltration and (M–P) fibrosis (orange arrows) of quadriceps. Glycoprotein and marker of ECM remodelling, fibronectin-1, was assessed in the quadriceps (black arrows) (Q–T). Extent of DMD phenotype was calculated (*mdx* AGG/*mdx* SED*100) to indicate extent of disease aggravation [13]. Data in B–E, I, M and Q are presented as mean \pm SEM and *n* are indicated by individual data points. Statistical analysis used one-way ANOVA: **P* < 0.05, ***P* < 0.01, ****P* < 0.001, *****P* < 0.0001. F–H, J–L, N–P, and R–T scale bar = 50 μ m.

do persist (weight gain, behavioural issues, adrenal suppression, cushingoid symptoms) due to blood-brain barrier penetration [10], indicating that non-steroid interventions may be better for long-term use.

We recently identified dimethyl fumarate (DMF), a drug with established safety data, prescribed for the autoimmune diseases, relapsing-remitting multiple sclerosis (MS) and psoriasis, as a potential corticosteroid alternative that could be rapidly repurposed for DMD based on acute treatment [11]. DMF is a potent immunoregulatory, anti-inflammatory and anti-oxidative drug via nuclear factor erythroid 2-related factor 2 (Nrf2) activation and hydroxycarboxylic acid receptor 2 (HCAR2) agonism [11] leading to suppression of molecular inflammatory signalling (i.e., nuclear factor kappa-light-chain-enhancer of activated B cells (NF- κ B)) and highly specific immunomodulation. Our proof-of-concept study in juvenile *mdx* mice undergoing a growth-dependent, muscle degenerative spike featuring hyper-inflammation and immune cell influx, demonstrated acute DMF treatment was more effective against key disease indices than SOC prednisone (PRED), including histopathology, muscle function, mitochondrial metabolism and disease driving gene signatures via Nrf2 signalling [12]. However, it is unclear whether these beneficial effects can be sustained with longer term treatment and, given the *mdx* mouse model manifests relatively mild disease compared to DMD patients [13], effective against more aggressive disease. Here, we used moderate exercise to aggravate disease and better recapitulate the DMD phenotype through which to scope DMF's efficacy and translational potential. We aimed to make a head-to-head comparison between DMF and SOC PRED as well as assess potential additive effects through combinatorial treatment.

2. Results

2.1. Exercise aggravation increases plasma CK levels and worsens dystrophic muscle histopathology

The dystrophic *mdx* mouse is the most used pre-clinical drug screening tool despite its relatively mild phenotype (Fig. 1A) compared to patients. Phenotype differences between sedentary (SED) WT and *mdx* mice are obvious at 8 weeks age, including elevated plasma (Fig. 1B) and skeletal (Fig. 1D–T) muscle damage indicators. We implemented TREAT-NMD's standard operating procedures to facilitate standardisation of our pre-clinical data to other laboratory groups for improved translational outcomes. Twice-weekly forced horizontal treadmill running from the age of 35 days was used to aggravate the *mdx* phenotype (Fig. 1A) according to TREAT-NMD SOP DMD_M.2.1.001 [14].

Exercise aggravation significantly increased plasma CK levels in *mdx* mice (Fig. 1B) but had no impact on endpoint forelimb (Fig. 1C) or whole-body grip strength (Supplemental Fig. 2A). While neither anthropometric measures nor respiratory or *ex vivo* force deficits were observed (Supplemental Fig. 2B–I), aggravation did exacerbate dystrophic histopathology. We analysed quadriceps, which are particularly recruited and damaged during exercise [15], and heart, to assess indices of muscle damage, inflammation, regeneration, immune cell infiltration, fibrosis and extracellular remodelling. Aggravation increased the unhealthy/healthy tissue ratio ($p = 0.0527$; Fig. 1D) and percentage of regenerating centronucleated fibres indicating greater muscle damage and repair activity (Fig. 1E–H), as well as CD68⁺ macrophage infiltration ($p = 0.0527$; Fig. 1I–L), mature fibrosis (Fig. 1M–P) and provisional matrix (Fig. 1Q–T) in *mdx* quadriceps. Perilipin-1+ adiposis of quadriceps muscle was not impacted by aggravation nor significantly different from WT (Supplemental Fig. 2J). Aggravation also did not affect active cardiomyocyte degeneration and fibrosis of the heart (Supplemental Fig. 2K–R) relative to *mdx* SED controls.

2.2. DMF improves grip strength and transcriptional control of myofibril assembly

DMF treatment increased forelimb grip strength (corrected for body weight) at the experimental endpoint (Fig. 2A) (notably, this measure was higher in *mdx* vehicle mice compared to WT (Fig. 1C)) but there was no effect of treatment on the hang test minimal holding impulse, which assesses both strength and endurance (Fig. 2B). Our functional data suggest that DMF might be better for preserving strength-based measures. Beyond these functional measures, we also investigated changes in body composition and found that in comparison to *mdx* vehicle, all treatments increased the fat mass index (Fig. 2C), which was reduced by ~40 % in *mdx* relative to WT mice (Supplemental Fig. 2B). Accordingly, we probed the muscle (quadriceps) transcriptome for genes associated with fatty acid metabolism. Of the 16 upregulated genes in *mdx* muscle (compared to WT), DMF downregulated 9 genes, PRED downregulated 2 genes and DMF + PRED downregulated 10 genes (Fig. 2D). Consistent with the known suppressive effects of PRED on muscle and bone growth [8,16], PRED treated alone, and in the DMF + PRED combination, significantly reduced the lean mass index relative to *mdx* vehicle (Fig. 2E). PRED reduced liver mass, and all treatments normalised the higher quadriceps mass noted in *mdx* aggravated (AGG) (and SED mice (Supplemental Tables 1 and 2) suggesting multi-tissue drivers of lean mass reduction.

At the experimental endpoint (8 weeks of age), EDL and soleus muscles, predominantly fast- and slow-twitch respectively, were harvested for *ex vivo* contractile testing. *Ex vivo* contraction measures were comparable between WT and *mdx* EDL and soleus (Supplemental Fig. 2H–I) thus there was no effect of treatments on either EDL or soleus absolute or specific force production (Fig. 2F–I). Only the DMF + PRED combination affected the force frequency relationship by increasing force production at 60 and 80Hz in the EDL (Supplemental Fig. 3A–B) and no treatment impacted fatigue or recovery measures (Supplemental Fig. 3C–D). We further probed transcriptional control of muscle contraction pathways for molecular changes in mixed fibre type muscle (i.e., quadriceps) that may be induced by treatments but not captured through *ex vivo* studies using fibre type exclusive/predominant muscles (i.e., EDL and soleus). Slow troponin isoforms, *Tnni1* and *Tnni3*, were significantly upregulated in *mdx* AGG compared to WT muscle (Fig. 2J), consistent with previous studies in dystrophic muscle [17]. The downregulation of *Actn2* by all treatments suggests concomitant sarcomere remodelling but only DMF and DMF + PRED treatment upregulated expression of *Tmod1*, *Neb*, and *Actn3* (and *Mybpc2* for DMF treatment), promoters of sarcomere stability [18,19] in the absence of dystrophin. PRED upregulated *Myh8*, a gene associated with regenerating DMD muscle [17]. There was no effect of treatment on plethysmography (respiratory) readouts (Supplemental Fig. 3E–G) or kyphosis index (Supplemental Fig. 3H–L), albeit these measures were unaffected by *mdx* aggravation.

2.3. DMF moderates the immune response in *mdx* quadriceps muscle

Persistent activation of the innate immune system leads to hyper-inflammation, oxidative stress and tissue damage in dystrophic muscles [7]. The unhealthy/healthy tissue ratio was significantly higher in *mdx* AGG quadriceps (Fig. 1D) but was not reduced by any drug treatment (Fig. 3A–C–F). However, there was a trend ($p = 0.0734$) for DMF to reduce the percentage of centronucleated regenerating fibres (Fig. 3B–F) suggesting modulation of degeneration/regeneration processes. Further investigation of the myogenic transcriptional pathway revealed that *Myog*, *Myod1*, *Tcf4*, *Mapk11* were upregulated in *mdx* AGG muscle. DMF downregulated *Myog* and *Mapk11*, PRED downregulated *Myod1* and *Mapk12*, and DMF + PRED combination downregulated *Tcf4* highlighting unique modulatory effects (Fig. 3G). Pan macrophage marker, CD68, was significantly reduced by DMF and PRED (Fig. 3H–L) consistent with their anti-inflammatory profiles. Interestingly, combined

--- WT levels

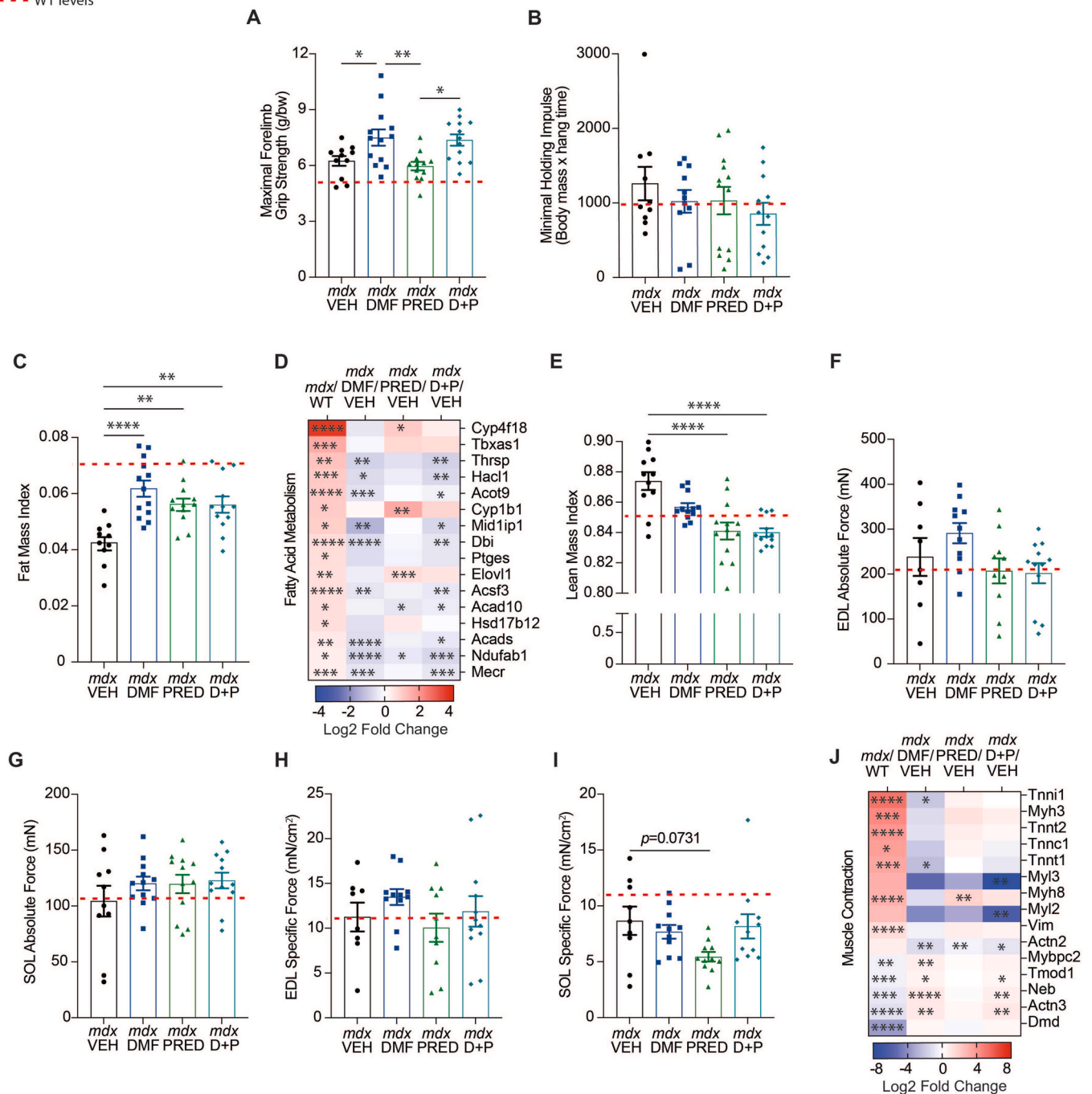


Fig. 2. DMF treatment improves grip strength and modulates transcriptional control of myofibril assembly. Functional parameters including (A) maximal forelimb grip strength and (B) minimal holding impulse (whole body grip strength). Anthropometric measures (C) fat mass index and associated transcriptional pathways (D) the fatty acid metabolism pathway, as well as (E) lean mass index was assessed. Absolute force was measured *ex vivo* in (F) EDL and (G) soleus and specific force was calculated (H–I). The transcriptomics dataset was probed for (J) muscle contractile associated genes. Data in D and J are based on log2 fold change from WT for *mdx* VEH and *mdx* VEH for treatment groups (DMF, PRED and DMF + PRED). Data in A–C, and E–I are presented as mean ± SEM and *n* are indicated by individual data points. Statistical significance was tested via one-way ANOVA: **P* < 0.05, ***P* < 0.01, ****P* < 0.001, *****P* < 0.0001.

delivery of DMF + PRED had no effect on macrophage infiltrate suggesting competing mechanisms of action in macrophages. Using western blot to gauge activation and protein expression of master inflammation regulator NF-κB in muscle, we showed that aggravation increased phosphorylation in *mdx* quadriceps (Fig. 3M), but that total protein expression levels were greater in *mdx* relative to WT muscles regardless (Fig. 3N). All treatments reduced both the NF-κB phosphorylation (Fig. 3M) and total protein expression (Fig. 3N) indicating comparable modulation of acute and chronic inflammation signalling via this

molecular mechanism. We also probed our transcriptomic dataset for common differentially expressed inflammatory markers associated with NF-κB induction and linked to human DMD pathomechanisms, including *Ccl2*, *Ccl6*, *Ccl7*, *Ccl8*, *Ccr2*, *Cx3cr1*, *Nfkb1*, *Nfkb2*, and *Nfkbib* [20–22] (Fig. 3O). 7 genes were significantly upregulated in *mdx* vehicle quadriceps and DMF treatment significantly downregulated 5 (*Ccl2*, *Ccl7*, *Ccl8*, *Ccr2*, and *Ccl6*) and trended to downregulate *Nfkb2* (*p* = 0.0702). Both PRED and DMF + PRED downregulated fewer inflammatory genes: one (*Cx3cr1*) and three (*Ccl7*, *Ccl2*, and *Ccr2*), respectively.

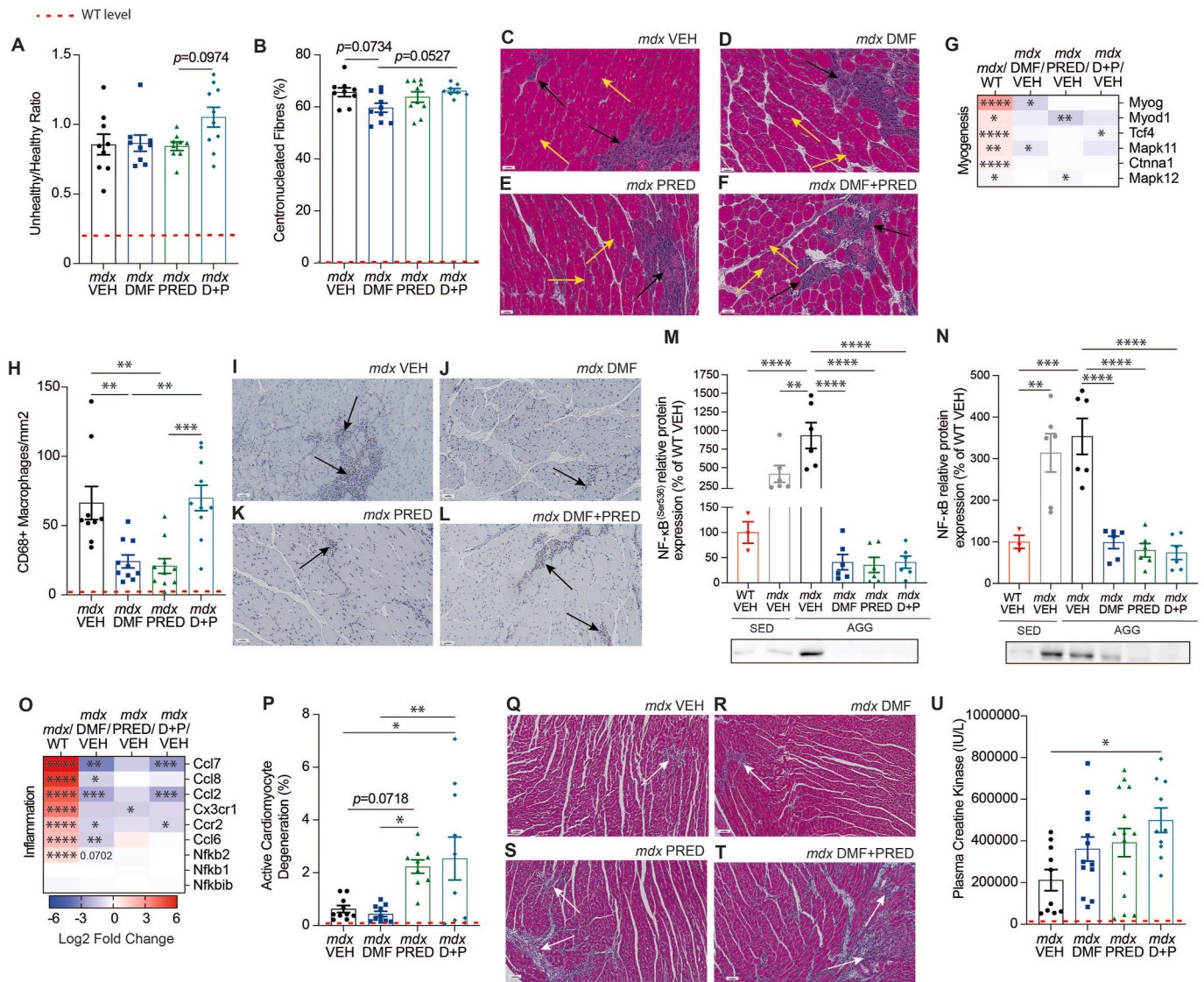


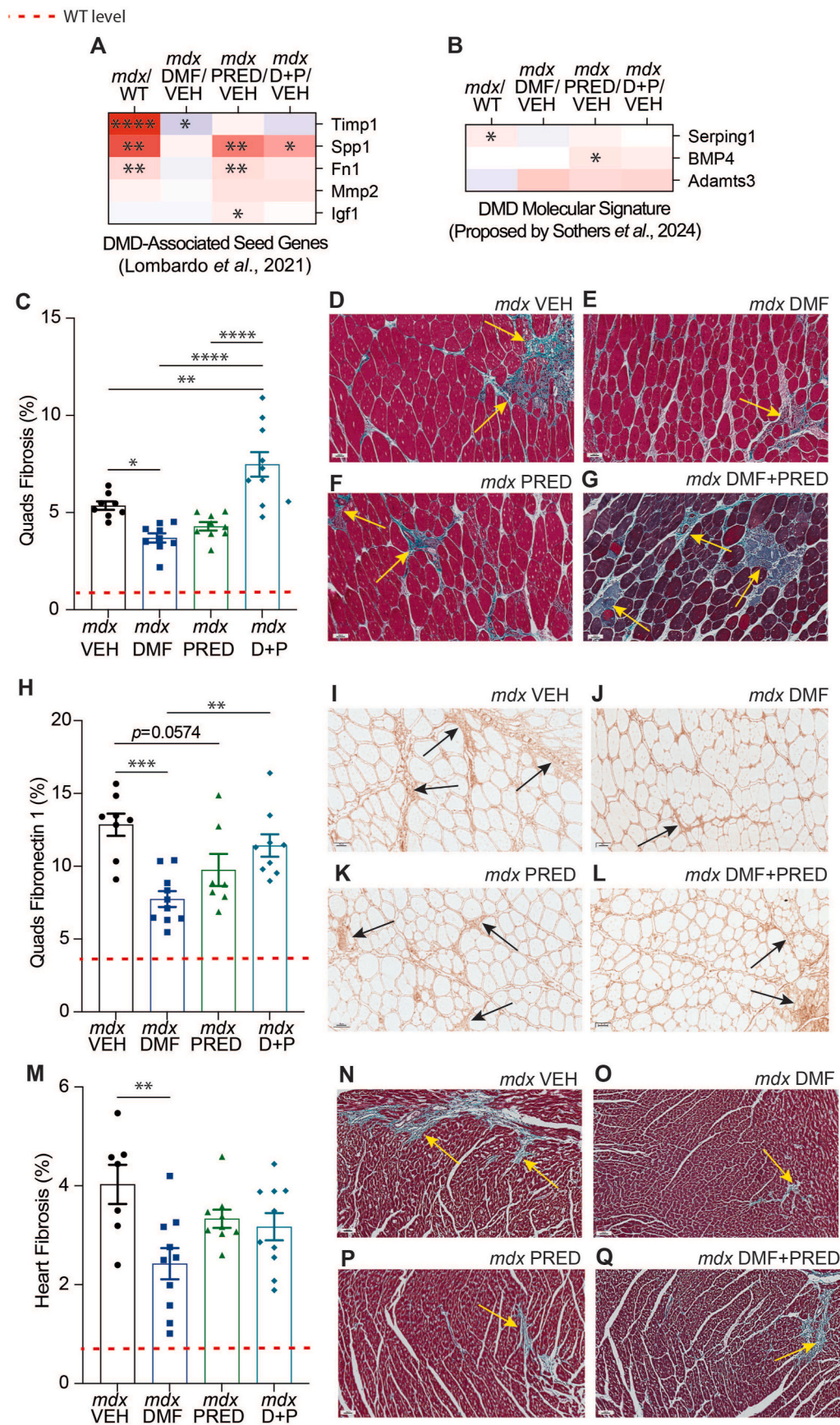
Fig. 3. DMF reduces inflammation and macrophage infiltration of quadriceps. The (A) unhealthy/healthy tissue ratio and (B) percentage of centronucleated fibres are shown in the quadriceps (C–F; yellow arrows indicate centronucleated fibres; black arrows indicate infiltrate). (G) Transcriptomic signature of myogenesis. (H) Pan macrophage marker CD68 was immunohistochemically assessed in the quadriceps and (I–L) representative images show CD68⁺ macrophages (indicated by black arrows). Protein expression of (M) phosphorylated and (N) total NF-κB in the gastrocnemius was quantified via Western blot. (O) The quadriceps transcriptomic dataset was probed for inflammatory markers commonly upregulated in DMD. (P) Degenerating area of the heart was also assessed via H&E and (Q–T) representative images show active cardiomyocyte degeneration (indicated by white arrows). (U) Clinically compatible biomarker creatine kinase was assessed at the experimental endpoint. Data in heatmaps (G and O) are based on log₂ fold change from WT for *mdx* VEH and *mdx* VEH for treatment groups (DMF, PRED and DMF + PRED). Data in A–B, H, M–N, P and U are presented as mean ± SEM and *n* are indicated by individual data points. Statistical significance was tested via one-way ANOVA: **P* < 0.05, ***P* < 0.01, ****P* < 0.001. C–F, I–L and Q–T scale bar = 50 μm.

Although cardiorespiratory decline is mostly evident in older *mdx* mice, we assessed heart histology since we aggravated our model and exercise has been shown previously to impact the heart of *mdx* mice [23]. Cardiomyocyte degeneration was greater in *mdx* hearts which DMF was unable to reduce. PRED trended to increase cardiomyocyte degeneration ($p = 0.0718$) and when combined DMF + PRED significantly increased this histopathologic feature (Fig. 3P–T). Endpoint plasma CK levels mirrored cardiac degeneration across the treatment groups (unchanged by DMF or PRED treatment but increased by combinatorial DMF + PRED) (Fig. 3U) suggesting CK is of cardiac origin.

2.4. DMF decreases fibrosis in the quadriceps and heart and downregulates key disease driving gene, *Timp1*

Fibrosis is a complex pathology that can result from increased ECM

synthesis and/or increased ECM degradation. In a recent meta-analysis, five genes were identified as candidate seed genes driving fibrosis within the DMD disease module (*Timp1*, *Spp1*, *Fn1*, *Mmp2*, and *Igf1*) [24]. A more recent study identified a *Bmp4*-induced molecular signature in DMD patient muscles involving upregulated expression of *Serping1*, *Adamts3*, *HCAR2*, *Smad8* and *Unc13c* [25]. We show that *Timp1*, *Spp1*, and *Fn1* (Fig. 4A) and *Serping1* (Fig. 4B) are upregulated in *mdx* AGG quadriceps alongside fibrosis (Fig. 4C–D). DMF treatment was effective at reducing *Timp1* (inhibitor of matrix metalloproteinases (MMPs)) gene expression (Fig. 4A) and histological fibrosis of quadriceps muscle (Fig. 4C and E). In contrast, PRED upregulated *Spp1*, *Fn1*, *Igf1* (a known effect of glucocorticoids [26–28]) and *Bmp4* transcription, and had no statistically significant effect on histological quadriceps fibrosis. In combinatorial DMF + PRED treatment, *Spp1* expression was increased (Fig. 4A) and histological fibrosis was worse than VEH treatment



(caption on next page)

Fig. 4. DMF reduces fibrosis of quadriceps and heart. Expression of the proposed (A) fibrosis-associated DMD seed genes [24] and (B) DMD molecular signature [25] was probed using our transcriptomic dataset. (C) Quadriceps fibrosis was quantified using Masson's trichrome staining and (D–G) representative images are shown. (H) Extracellular matrix remodelling was assessed via staining for the glycoprotein fibronectin 1 and (I–L) representative images are shown. Fibrotic area of the heart was also assessed and (M–Q) representative images are shown. Data in heatmaps (A–B) are based on log₂ fold change from WT for *mdx* VEH and *mdx* VEH for treatment groups (DMF, PRED and DMF + PRED). Data in C, H and M are presented as mean ± SEM and *n* are indicated by individual data points. Statistical significance was tested via one-way ANOVA: **P* < 0.05, ***P* < 0.01, ****P* < 0.001, *****P* < 0.0001. D–G, I–L and N–Q scale bar = 50 mm.

(Fig. 4C–F–G). Fibronectin 1 is a glycoprotein in the ECM that modulates cell behaviour relevant to inflammation and regeneration [29], it provides structural support, facilitates satellite cell activation, and promotes myoblast fusion during skeletal muscle repair. Although fibronectin 1 plays a vital role in regeneration by acting as a scaffold for cellular migration and ECM remodelling, its dysregulation can lead to fibrosis and subsequent impaired muscle function. DMF was the only drug to significantly reduce fibronectin levels in quadriceps, although PRED did trend (*p* = 0.0574) to reduce it compared to VEH treatment (Fig. 4H–L). DMF was also the only drug to reduce cardiac fibrosis (Fig. 4M–Q) consistent with its anti-fibrotic effects in quadriceps (Fig. 4C and H).

2.5. DMF reduces muscle adiposis through modulation of the adipogenic and sphingolipid metabolism transcription programs in *mdx* muscle

Replacement of muscle fibres with adipose tissue is prominent in human DMD muscle but minimal in *mdx* muscle, i.e., perilipin-1, a protein that localises to adipocytes, was comparable between WT and *mdx* quadriceps (Supplemental Fig. 2J). Nevertheless, DMF treatment decreased adipocyte abundance whereas PRED, alone and in combination with DMF, had no effect (Fig. 5A–E). To interrogate the potential underlying mechanisms, we probed lipid metabolism and fibro-adipogenic progenitor (FAP)-related pathways in our transcriptomics dataset. Of the 3 established FAP-associated marker genes in humans, (*Cd34*, *Pdgfra*, and *Dcn*), *Cd34* expression was upregulated in *mdx* quadriceps and was downregulated by DMF (Fig. 5F). Reactome pathway analysis (Supplemental Table 3) revealed that the tumour necrosis factor receptor (TNFR)-mediated ceramide production pathway was significantly upregulated in *mdx* quadriceps and was normalised by DMF but not PRED treatment. We probed genes within this pathway (Fig. 5G) and revealed DMF normalised *Tnfrsf1a* (a pro-inflammatory biomarker in human DMD [30]) and *Nsmaf* expression. The *Nsmaf* gene encodes a protein involved in sphingolipid metabolism, specifically regulating the enzyme neutral sphingomyelinase (nSMase), contributing to muscle cell membrane repair and regulation of inflammation and regeneration [31]. Sphingolipid metabolism pathways were also probed since DMF is known to modulate sphingolipids through HCAR2 agonism in the context of MS [32]. Of the 11 upregulated sphingolipid metabolism genes identified in *mdx* muscle, DMF downregulated 2 while PRED and DMF + PRED significantly upregulated 9 and 5 genes, respectively (Fig. 5H). Furthermore, DMF normalised the expression of *Sgms1* and *Cers1*, which were downregulated in *mdx* quadriceps. Ten adipogenesis genes were differentially expressed in *mdx* muscle: 4 upregulated and 6 downregulated (Fig. 5I). DMF was more effective at moderating the adipogenic gene program than PRED mono or combination therapy.

2.6. DMF significantly recovers inflammatory, fibrosis and fat mass associated parameters

The recovery score is used to express the effect of a treatment, not just by the difference between treated and untreated *mdx* mice, but relative to the extent of the deficiency between WT and *mdx* mice [13]. We calculated the recovery score (Fig. 6) of parameters that were significantly recovered by treatment. DMF, PRED and DMF + PRED normalised protein expression of NF-κB phosphorylated (108 %, 109 % and 108 %, respectively) and total (110 %, 119 % and 122 %,

respectively). CD68 macrophage infiltration of quadriceps was improved by both DMF and PRED to a similar extent (65 % vs. 66 %, respectively) whilst DMF + PRED showed no improvement (0.78 %). Percentage of quadriceps fibronectin 1 was improved by both DMF and PRED (61 % vs 37 %, respectively) and while DMF + PRED improved the recovery score (17 %), this was significantly less than when DMF was delivered alone. Fat mass index was recovered by 59 %, 38 % and 34 % following DMF, PRED and DMF + PRED treatment, respectively. DMF was the most effective treatment at recovering cardiac fibrosis (46 %) followed by PRED and DMF + PRED, which had a comparable recovery score approximately half that of DMFs (20 % and 24 %, respectively). Similarly, DMF (37 %) and PRED (23 %) recovered quadriceps fibrosis whilst DMF + PRED worsened fibrosis resulting in a negative recovery score (−47 %), which may be linked to the cancelling effect of the combined drugs on macrophage infiltration.

2.7. DMF transcribes a highly specific anti-inflammatory and anti-oxidation signature in muscle

A well-established mechanism of action (MOA) of DMF is via activation of Nrf2, which initiates a potent cytoprotective response (Fig. 7A). Deep transcriptome profiling did not reveal changes to expression of *Nf2el2* (Nrf2), or its negative repressor, *Keap1*, in response to DMF treatment. However, DMF normalised the otherwise upregulated expression of proteasomal subunit genes, *Psmb1*, *Psmc1*, *Psmc4*, and *Psmc1* (Fig. 7B), which degrade Nrf2 and prevent its activity. DMF also tempered expression of antioxidant/detoxification enzymes *Ccs*, *Prdx2*, and *Txn2* (Fig. 7C). Consistent with the transcriptomic profiling, protein expression of Nrf2, Keap1 and NQO1 were comparable between the *mdx* vehicle and treatment groups (Fig. 7D–F) whilst DMF + PRED significantly decreased SOD1 expression (Fig. 7G). It should be noted that, except for Keap1, where expression was increased in the *mdx* VEH SED mice compared to WT, no other genotype differences were observed in the first instance.

To explore the possibility that Nrf2 activity may be regulated downstream of its expression or stability, we examined transcriptomic changes in known repressors of antioxidant response element (ARE)-driven transcription (Fig. 7H). *Fosl2* a transcriptional repressor of the Nrf2-ARE signaling pathway was upregulated in *mdx* muscle whereas *Sqstm1* was downregulated. Inside the nucleus, Nrf2 is competitively inhibited by several protein complexes. Nrf2 forms a heterodimer with sMAF proteins, enabling ARE binding and activation of antioxidant gene transcription [33]. Bach1 and Bach2, members of the Cap 'n' Collar (CNC) basic leucine zipper (b-Zip) family, like Nrf2, also bind sMAF to form a heterodimer capable of recognizing AREs [34]. Thus, Bach1 and 2 compete with Nrf2 on two levels: first, by binding to sMAF and second, by occupying AREs. Unlike the Nrf2-sMAF complex, which activates transcription, the Bach1/2-sMAF complex functions primarily as a transcriptional repressor of antioxidant genes [35]. In our study, expression of *Bach1* was significantly increased in all treatment groups whereas *Bach2* expression increased only in the combined DMF + PRED treatment group. DMF treatment significantly increased *Bach1* expression levels in *mdx* mice (Fig. 7H) suggesting that Nrf2 activity is tempered by competition with Bach1 for binding sites. Although *Bach1* expression was significantly reduced in untreated *mdx* mice, there was no indication of Nrf2 expression (e.g., protein expression of Nrf2 or Phase I antioxidants). Rather, there was significant upregulation of nuclear receptor repressors, which inhibit Nrf2 activity by preventing its

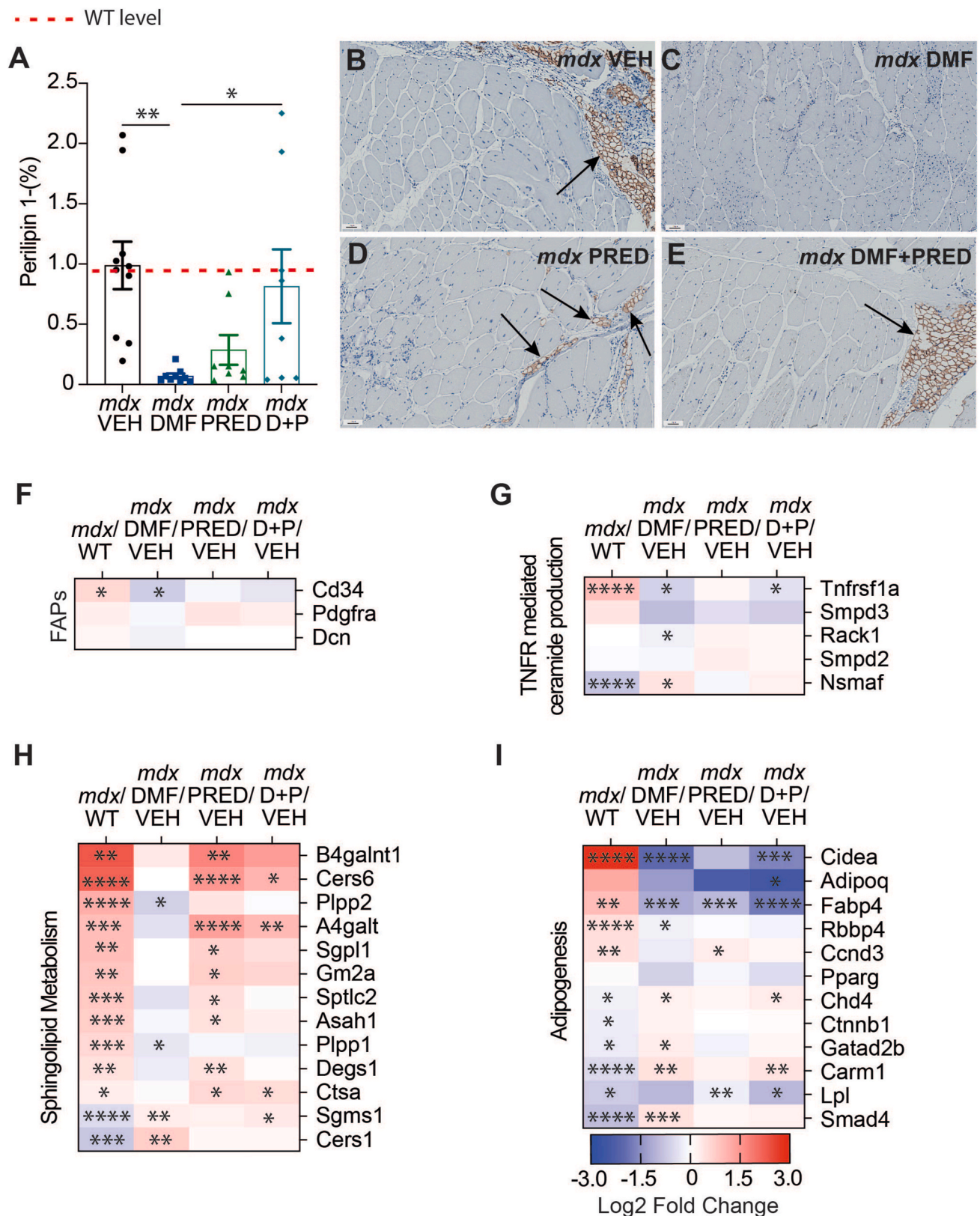


Fig. 5. DMF decreases muscle lipid content through modulation of adipogenesis and sphingolipid metabolism pathways in quadriceps. (A–E) Percentage of perilipin-1+ lipid droplets in quadriceps. Lipid associated transcriptional pathways were probed including (F) FAPs, (G) TNFR mediated ceramide production, which was a significantly altered Reactome pathway in *mdx* aggravated (AGG) relative to WT quadriceps, (H) sphingolipid metabolism and (I) adipogenesis. Data in all heatmaps (F–I) are based on log₂ fold change from WT for *mdx* VEH and *mdx* VEH for treatment groups (DMF, PRED and DMF + PRED). Data in (A) is presented as mean ± SEM and *n* are indicated by individual data points. Statistical significance was tested via one-way ANOVA: **P* < 0.05, ***P* < 0.01, ****P* < 0.001, *****P* < 0.0001. B–E Scale bar = 50 μm.

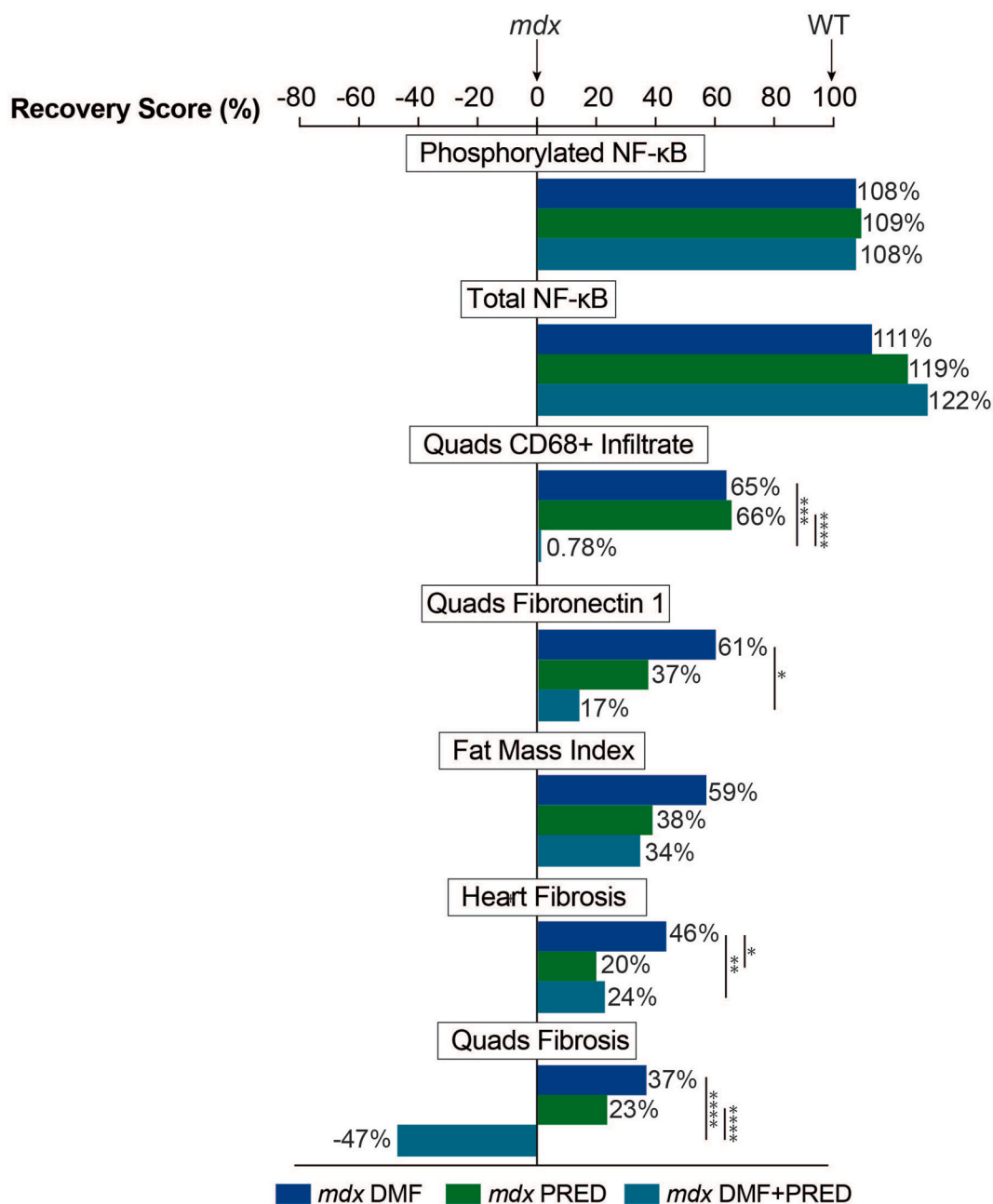


Fig. 6. The impact of the treatments on the *mdx* mouse. The recovery score is used to express the effect of a treatment, not just by the difference between treated and untreated *mdx* mice, but relative to the extent of the deficiency between WT and *mdx* mice. A recovery score of 100 % indicates the parameter is equal to that of the WT while a score of 0 % indicates no improvement has been made. This was calculated as $(mdx \text{ treated}) - (mdx \text{ untreated}) / (WT) - (mdx \text{ untreated}) \times 100$ [13].

binding to the ARE [36]. For example, expression of nuclear receptor, retinoic acid receptor alpha (*Rara*), was increased whereas expression of estrogen receptor 1 (*Esr1*) was reduced in *mdx* relative to WT muscle. Gene expression of estrogen related receptor beta (*Esr2*) and *Rara* receptors were decreased by all treatments whereas expression of *Esr1* was significantly increased by DMF and PRED treatment. To illustrate this regulatory complexity, a mechanistic schematic is presented, highlighting how Bach1 and (RAR α), in particular, may interfere with Nrf2-small Maf (sMAF) protein binding and ARE engagement to maintain rheostatic control of Nrf2 activation with longer term DMF treatment.

3. Discussion

Our methodological approach of twice weekly forced treadmill running was successful to increase clinically relevant muscle damage biomarker, plasma CK, and histopathological hallmarks in hindlimb quadriceps muscle. Cardiorespiratory phenotypes are usually only evident from ~12 to 18 months age in *mdx* mice [1] and it was encouraging that early cardiac muscle degeneration and fibrosis were induced by exercise aggravation. Increasing the frequency (e.g., thrice weekly running), duration (e.g., >20 min per session) or difficulty (e.g., downhill running) of the exercise regimen could further induce both histopathological and functional phenotypes across all impacted physiological systems in future work.

Our data highlight that DMF's MOA over the moderate term involves

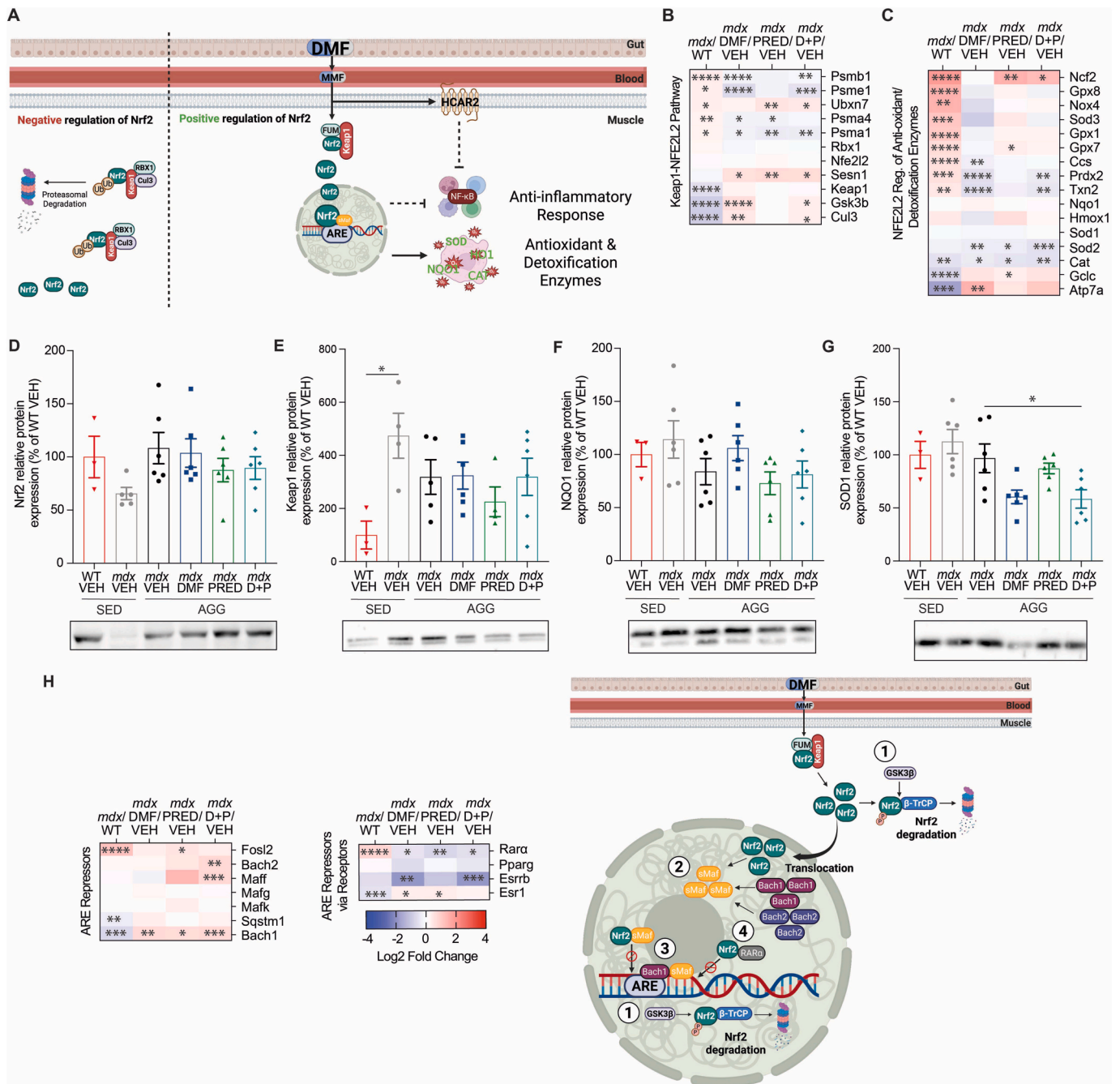


Fig. 7. DMF treatment tempers expression of detoxification enzymes in muscle. (A) DMFs MOA involves dual anti-inflammatory and -oxidative function through transcription of Nrf2. The muscle transcriptome was probed for molecular pathways involved in DMF's MOA including the (B) Keap1-Nrf2 pathway and (C) Nrf2 regulation of antioxidant/detoxification enzymes pathway. Protein expression of (D) Nrf2, (E) Keap1, (F) NQO1 and (G) SOD1 was quantified via western blot. The muscle transcriptome was also probed for (H) non-receptor antioxidant response element (ARE) repressors and ARE repressors via receptors. A diagrammatic representation of Nrf2-ARE inhibition pathway demonstrates [1] GSK-3b mediated Nrf2 phosphorylation and degradation in the cytoplasm and nucleus [2]; competitive inhibition of Nrf2 binding with small Maf proteins (sMAF) and [3] competitive inhibition of Nrf2-sMAF with the Bach1/2-sMAF heterodimer which prevents Nrf2 binding to the ARE [4]; interaction of RAR α with Nrf2 inhibiting binding to the ARE. Heatmap data (B–C and H) are based on log₂ fold change from WT for *mdx* VEH and *mdx* VEH for treatment groups (DMF, PRED and DMF + PRED). Data in D–G are presented as mean \pm SEM and *n* are indicated by individual data points. Statistical significance was tested via one-way ANOVA: **p* < 0.05, ***p* < 0.01, ****p* < 0.001, *****p* < 0.0001.

highly specific immune modulation, likely via Nrf2 activity, HCAR2 agonism or both. We show that DMF was able to recover histopathological exacerbations induced by aggravation of the *mdx* phenotype by on average, 50 % (Fig. 6). In contrast, PRED recovered on average, 26 %. DMF is twice as effective at treating these measures, and from a safety standpoint, could be better since it does not reduce lean tissue mass like PRED. In our short-term DMF screen, we demonstrated Nrf2 activation

via increased expression of Phase II antioxidant enzymes, NQO1 and SOD1 [12], the biomarkers of DMF's MOA and efficacy in MS. However, in this study, moderate-term DMF treatment did not maintain Nrf2, NQO1 or SOD1 upregulation (transcriptionally or at the protein level) (Fig. 7). DMF likely induces temporal Nrf2 activation in response to environmental (oxidant, inflammation) cues to maintain a proportionate antioxidant defense system. For example, GSK-3b (glycogen synthase

kinase 3b) phosphorylates Nrf2 resulting in its nuclear and cytoplasmic degradation independent of Keap1 [37] – *Gsk3b* transcription was increased by DMF treatment (alone and in combination with PRED; Fig. 7B). Furthermore, gene expression of several nuclear repressors of Nrf2-ARE transcription were altered by DMF (e.g., *Bach 1*, several receptor repressors). Our data support activation of an oxidant sensitive override mechanism to avoid hyper-Nrf2-activation. This mechanism appears to interplay strongly with quenching of NF- κ B mediated inflammation, suggesting immune cells are the predominate source of ROS in DMD. Clearly, Nrf2 signaling is highly regulated through a complex network of interactions. Much of this regulation operates through rheostatic negative feedback loops, where the activation of antioxidant responses eventually leads to suppression of the initial signal to restore homeostasis [35].

The most striking effect of DMF in our study was reducing fibrosis of the heart and quadriceps although it is important to note that fibrosis was mild in our 8-week-old *mdx* mice (~4–5 %, consistent with others [38,39]) even with exercise aggravation. The cardioprotective effect of DMF is particularly important given the high prevalence of cardiomyopathy in DMD and its contribution to disease progression and mortality [40,41]. Although the degree of cardiac pathology is subtle at this age, the finding that DMF can modulate myocardial fibrosis suggests potential for therapeutic benefit in older or more severely affected models. Recently, in skeletal muscle we showed DMF could modulate fibrosis-associated seed genes (*Mmp2*, *Spp1*, and *Timp1*) [12] that drive the DMD disease program described by Lombardo et al. [24]. Here we show that moderate-term DMF treatment sustains *Timp1* suppression, whilst PRED significantly upregulates expression of 3 seed genes (*Spp1*, *Fnl1*, and *Igf1*). DMF downregulated key genes involved in collagen formation, ECM degradation and organisation whilst PRED significantly upregulated over more than half (34 out of 54 differentially expressed genes). DMF was previously shown to ameliorate lung [42] and renal [43] fibrosis indicating systemic anti-fibrotic function. Early in tissue repair, fibronectin 1 is a crucial component of the provisional ECM, promoting fibroblast recruitment, myoblast adhesion, and signalling for ECM assembly [29]. However, when dysregulated, fibronectin 1 drives excessive ECM deposition, where provisional matrix transitions into a mature, collagen-rich fibrotic matrix (stained blue by Masson's trichrome). Here we showed that DMF was the only treatment to decrease fibronectin 1 in the quadriceps (Fig. 4H), consistent with the decrease in histological fibrosis observed (Fig. 4C). Of the several possible molecular mechanisms regulating DMFs anti-fibrotic effect, our data indicate reduced (CD68⁺) macrophage recruitment/accumulation/transition and NF- κ B protein expression are central. We saw no evidence of DMF-dependent inhibition of TGF- β /Smad3 signalling or *Spp1*/osteopontin expression. Notably, when treated in combination, DMF + PRED exacerbated exclusively quadriceps fibrosis (–47 % recovery score). This effect could be a result of over-immunosuppression teamed with activation (i.e., by treadmill running) strain highlighting the intricate symphony of immunology required to maintain muscle over fibrotic tissue. As a weight-bearing and high force generating muscle group, quadriceps are more prone to damage than the heart and therefore seem more sensitive to the detrimental effect of over-immunosuppression. This aspect requires careful consideration in the planning of future clinical trials testing DMF and other immunomodulatory/anti-fibrotic agents for DMD where SOC may need to be withheld, or exclusively steroid naïve participants recruited.

In the context of human MS, DMF is known to re-program fat metabolism, especially sphingolipid metabolism [32]. Transcripts of the sphingolipid *de novo* biosynthesis pathway are upregulated in skeletal muscle of patients with DMD as well as in other muscular dystrophies [44]. Our data highlight multiple points of control of systemic and muscle-specific adipose tissue content. *Mdx* mice (SED and AGG) are particularly lean (low fat mass index relative to WT) and our transcriptomic data point to increased metabolic demand as a mechanism [45]. DMF treatment normalised these transcriptomic signatures and the

fat mass of *mdx* animals. The primary active metabolite of DMF, monomethyl fumarate, is a ligand for HCAR2 which is highly expressed on adipocytes and immune cells [46]. HCAR2 agonism prevents lipolysis through inhibition of adipose triglyceride and hormone sensitive lipases [32]. In contrast to these systemic effects, DMF reduced adipocyte abundance (perilipin-1) at the muscle level in *mdx* mice. Via its distinct immunomodulatory effects on macrophage sub-populations, DMF downregulated FAP-associated marker genes, which is important because a subset of FAPs can undergo adipogenic differentiation contributing to fatty infiltration of human DMD muscle [47]. DMF also reduced *Tnfrsf1a* transcripts which were upregulated in *mdx* muscle. In humans, TNFR1 agonism contributes to muscle adiposis by inducing sphingomyelin hydrolysis-mediated ceramide production. Ceramides are bioactive molecules capable of activating apoptotic and pro-inflammatory pathways and their accumulation in muscle is linked to myopathy [48]. Consistent with a study by Laurila et al. [44] in *mdx* mice, we show that the sphingolipid metabolism pathway is upregulated in dystrophic muscle. Although DMF downregulated only 2 of 10 significantly upregulated genes within this pathway, PRED led to further upregulation of 9 genes. Sphingolipid metabolism is heightened in MS resulting in ceramide production [49] and more recently, sphingosine-1-phosphate (S1P), as well as transcripts of other sphingolipids were shown to be highly upregulated in dystrophic human and *mdx* muscle [50]. Muscle adiposity is much more problematic in human than *mdx* DMD [51], as is obesity [52]. Whether DMF will be efficient enough in humans given that the adipose pathology is worse is an important translational question for follow up. If it were to be similarly effective against human DMD muscle adiposis, DMF could be a strong candidate for repurposing with potential added benefits over standard of care PRED.

Our study reveals important translational aspects. Firstly, immune system involvement in DMD progression is complex as is its pharmacological control. Timely and successful muscle regeneration and repair is highly dependent on a well-regulated inflammatory cascade – chronic inflammation and cytokine signalling can promote macrophage phenotype shifts and muscle pathology, while over-immunosuppression can dysregulate muscle regeneration [53]. Alone, DMF and PRED share similar anti-inflammatory and immunomodulatory capability (transcriptionally) to effectively reduce macrophage infiltration of muscle. We showed previously that with short-term treatment, DMF activates Nrf2 signalling in the muscle [12]. However, moderate-term treatment in our aggravated model indicates anti-inflammation via Nrf2-independent inhibition of NF- κ B expression and activation is the principal MOA. We propose this effect is driven by HCAR2 agonism. Corticosteroids similarly repress NF- κ B signalling as their principal MOA, albeit via activation of the glucocorticoid receptor which is also responsible for their side-effects [8]. From a translational perspective, DMF could be a relevant PRED surrogate to slow DMD progression on this point alone. Indeed, some 37 % of American DMD patients are corticosteroid naïve with 25 % never commencing therapy and 12 % having discontinued [9]. Side-effects were reported as the main reason for rejection of pharmacological standard care in 65 % of these patients [9]. These data indicate an unmet need for efficient, non-steroidal anti-inflammatories with at least comparable efficacy to corticosteroids.

In summary, our data highlight DMF as a promising translational candidate for DMD with a potentially better safety profile than glucocorticoids. Importantly, DMF is already approved for the treatment of MS and psoriasis and continues to demonstrate long-term safety and clinical efficacy in both controlled trials and real-world settings [54,55] reinforcing its relevance for inflammatory-driven diseases. However, it is also important to acknowledge that DMF has not shown consistent clinical efficacy across all conditions. For example, it failed to demonstrate benefit in a recent amyotrophic lateral sclerosis (ALS) clinical trial [56] highlighting that translational success is not guaranteed and must be evaluated within each disease framework. Further, there are translational limitations imposed by the *mdx* mouse model which although

widely used in DMD research, portrays a relatively mild phenotype and disease progression compared with patients. Model selection is critical in preclinical DMD research, and we anticipated that our aggravation protocol would induce a more human comparable phenotype than it did. The use of aged *mdx* mice, which do show human relevant characteristics particularly regarding fibrosis and loss of function, will be crucial for well-informed clinical translation decisions. Our follow-up study (AFM24216) due for completion in 2025 intends to confirm longitudinal, disease modifying capacity as a final hurdle to clinical translation. Moderate-term DMF demonstrated anti-inflammatory, anti-fibrotic, and anti-lipogenic effects against the mild DMD phenotype of 8-week-old exercise aggravated *mdx* mice. A strong point of our study was the inclusion of a combinatorial DMF + PRED group to survey potential drug interactions. Worsening of skeletal muscle fibrosis with combined treatment suggests careful consideration of dose and dosing regimen will be needed during clinical trial design to ensure over-immunosuppression does not exacerbate disease. We propose DMF could be a useful corticosteroid alternative for the vast DMD patient population who outright reject, or have discontinued, corticosteroid use.

4. Materials and methods

4.1. Animals

Male C57BL/10ScSnJ (wild-type (WT)) and dystrophin-deficient C57BL/10ScSn-*Dmd*^{*mdx*}/J (*mdx*) mice were bred at Western Centre for Health, Research and Education (Sunshine Hospital, Victoria, Australia). Given that DMD is an X-linked disorder, only male mice were utilised in this study. Animals were housed on a 12:12 h light-dark cycle at 20–25 °C and 40 % humidity. Litters were weaned at 21 days of age and randomly assigned to cages (up to 4/cage). Food and water consumption was monitored weekly.

4.2. Treatment

Mdx mice were randomly assigned to treatment groups at 21 days of age [1]: 0.5 % methylcellulose (vehicle (VEH)) [2], DMF [3], PRED or [4] a DMF and PRED (DMF + PRED) combination (all treatments suspended in vehicle). WT mice were treated with the 0.5 % methylcellulose VEH. Animals were weighed and treated daily up until 8 weeks of age via oral gavage. Treatments were prepared relative to individual body weights to give a final daily dosage of 100 mg kg⁻¹/day DMF, 5 mg kg⁻¹/day PRED or 100 mg kg⁻¹/day DMF with 5 mg kg⁻¹/day PRED. Selected dosages are consistent with our previous study [12], which aligns with pre-clinical studies assessing DMF for MS [57] and work by Manico et al. [58] who pre-clinically used this PRED dosage in *mdx* mice. There was no impact of any treatment on body weight or food and water consumption in *mdx* mice (Supplemental Fig. 1A–D).

4.3. Treadmill exercise-aggravation protocol

The *mdx* mouse is a useful pre-clinical therapeutic screening tool but presents with challenges that may compromise translational outcomes later in the drug development pipeline. After an initial acute degenerative period during rapid maturational growth at ~3–5 weeks age, the disease stabilises into relatively mild cyclical degeneration and regeneration bouts across the lifespan until ~12 months age when disease progression escalates [13]. Applied exercise exacerbates muscle dystrophy in the *mdx* mouse, particularly fibrosis and subsequent lipid infiltration [15]. From 4 weeks of age, mice in the aggravated (AGG) cohort were subjected to a 30 min run on a horizontal treadmill (PanLab Harvard Bioscience) at 12 m/min, twice-weekly based on a protocol developed by TREAT-NMD (SOP DMD_M.2.1.001) [14]. All animals were exercised in a temperature and light controlled environment and the exercise was performed with constant monitoring. A forced treadmill run to fatigue, starting at 5 m/min speed for 5 min and increasing by 1

m/min thereafter, was substituted for the final treadmill run and was undertaken 3 days prior to the experimental endpoint.

4.4. Functional muscle strength

Forelimb and whole-body grip strength was assessed weekly as previously stated [12]. All functional testing was performed blinded, by the same experimenter.

4.5. Respiratory function

Respiratory function was assessed once at the experimental endpoint at 8 weeks of age in conscious, unrestrained mice using a whole-body, non-invasive plethysmograph (WBP; Data Sciences International, USA). The plethysmograph and bias flow regulator were calibrated prior to the run. Mice were placed in one of the four plethysmograph chambers and acclimated for 30 min. Thereafter, respiratory measurements were collected using Buxco FinePointe software over a 15 min period.

4.6. Body composition analysis

At 8 weeks of age, body composition was analysed using the EchoMRI-100H scanner (EchoMRI, Houston, USA) as conducted by us previously [59].

4.7. Kyphosis index

Prior to endpoint, at 8 weeks of age, animals were lightly anaesthetised (2.5 % isoflurane) and X-rayed in an IVIS Lumina X5 (PerkinElmer). Images were acquired with Living Image(R) 4.8.0 (64bit) using photograph (medium binning, F/stop 6) and X-ray (high resolution binning, F/stop 6) overlay. Images were imported into ImageJ and the kyphosis index was calculated from a line drawn between the C7 vertebra to L6 (usually corresponding with the posterior edge of the iliac wing; line AB) divided by a line perpendicular to this from the dorsal edge of the vertebra at the point of greatest curvature (line CD) [60].

4.8. Plasma creatine kinase

Blood was collected from the endpoint surgery via cardiac puncture into Greiner Bio-One 0.5 ml lithium heparin tubes. Plasma was separated via centrifugation (5 min, 3000×g, 4 °C). Creatine kinase (CK) units were quantitated spectrophotometrically (CK-NAC kit, Randox Laboratories, UK) [12].

4.9. Surgical procedure

At the experimental endpoint, animals were weighed, treated via gavage, and then deeply anaesthetised (4 % induction and 2.5 % maintenance isoflurane). The left extensor digitorum longus (EDL) and soleus were tied tendon to tendon with suture thread and excised for *ex vivo* contractile experimentation. Other muscles and organs were excised and snap frozen to be weighed later (refer to Supplemental Tables 1 and 2).

4.10. Ex vivo contractile function

After excision, the proximal ends of the EDL and soleus muscles were placed onto a force transducer and the distal end fixed to a micromanipulator in organ baths (Danish Myo Technology, Hinnerup, Denmark) via knotted loops. In depth information regarding the contractile protocol has previously been described by our lab group [12]. Outcome measures included specific/absolute force, force frequency, fatigue, and recovery.

4.11. Histological analyses of the quadriceps and heart

The right quadriceps and hearts were initially snap frozen then later slow thawed at 4 °C in 10 % neutral buffered formalin for 48 h. Following fixation, quadriceps and hearts were transferred to 70 % ethanol until paraffin embedding. Sections were cut at 5 µm thick for the quadriceps and heart. Hearts were cut diagonally at the mid-ventricle. Sections were stained and assessed as detailed below. All assessments were performed on blinded images by the same experimenter. Full cross-sectional areas were imaged at 1X using a Zeiss Axio Imager Z2 microscope (Carl Zeiss MicroImaging, GmbH, Germany).

4.11.1. Haematoxylin and eosin (H&E)

Quadriceps and hearts were stained with H&E [61]. For quantification of unhealthy/healthy tissue ratio in the quadriceps, the H&E colour deconvolution plugin on ImageJ was used. The eosin component (normal, undamaged myofibres) was measured via thresholding (TREAT-NMD SOP: DMD_M.1.2.007) [62]. The proportion of centronucleated fibres in the quadriceps was calculated by analysing ~200 fibres per section [63]. For active cardiomyocyte degeneration of the heart, degenerating tissue and clusters of inflammatory infiltrate were measured and expressed relative to the total area [41].

4.11.2. Masson's trichrome

Masson's trichrome was used to assess collagen/fibrotic connective tissue content in the quadriceps and heart. Analysis of the percent area of fibrosis in both the quadriceps and heart was conducted using the Masson's colour deconvolution plugin on ImageJ [23].

4.11.3. Immunohistochemistry

To quantify macrophage and adipocyte infiltration, anti-CD68 (ab125212) and perilipin-1 (9349S) primary antibodies were utilised at a dilution of 1:500 and 1:200, respectively and stained as described by us previously [12]. CD68 positive macrophages were manually counted using DotDotGoose (version 1.7.0) and expressed as number per square millimetre of muscle cross section as measured via ImageJ. Adipocytes were manually traced using ImageJ and expressed as percentage of the total area. Similarly, to evaluate the content in the ECM glycoprotein fibronectin 1, anti-fibronectin (ab2413) primary antibody was utilised at a dilution of 1:200 and expressed relative to the total area.

4.12. Transcriptomics

4.12.1. Ribonucleic acid (RNA) extractions, quantification, and integrity

Frozen quadriceps muscles (10–15 mg; $n = 10$ per group) were removed from -80°C storage where extractions were performed using the AllPrep Deoxyribonucleic acid (DNA)/RNA/microRNA (miRNA) Universal Kit (Qiagen, Valencia, USA) which includes a genomic DNA elimination step to remove DNA from total RNA. Aliquots were taken for RNA quantification and integrity assessment using a Nanodrop spectrophotometer (Thermo Fisher Scientific). 1 µl of sample was placed on the instrument and readings for RNA concentration (ng/µl), the A260/280 ratio, and A260/230 ratio were recorded. Samples were diluted to 100 ± 20 ng/µl and RNA integrity was assessed using a TapeStation System 4150 (Agilent Technologies, USA). An RNA quality indicator score greater than 7 was considered intact and of high integrity [64].

4.12.2. RNA sequencing

The library construction and RNA sequencing were performed by Beijing Genomics Institute (Shenzhen, China) and ~1 µg total RNA was used for library construction. For library preparation, samples were denatured, and mRNA was enriched using oligo (dT) attached magnetic beads. The messenger RNA (mRNA) was fragmented into small pieces and the double strand complementary DNA (cDNA) was synthesised. These double-stranded cDNA fragments were subjected to end-repair and a single 'A' nucleotide is added to the 3' ends of the blunt

fragments and subsequently ligated to the adapter. The ligation product was purified and enriched with polymerase chain reaction (PCR) amplification to yield the final cDNA library. Sufficient quality DNA nanoballs (DNBs) were loaded into patterned nanoarrays using a high-intensity DNA nanochip technique and sequenced through combinatorial Probe-Anchor Synthesis (cPAS).

4.12.3. Bioinformatics

FASTQ files were processed using the NfCore/RNAseq (v3.10.1) pipeline [65]. Reads were aligned to the *Mus musculus* Ensembl GRCm39.release-109 reference genome using STAR aligner [66] and quantified using Salmon [67] producing raw genes count matrix. Various quality control metrics were generated and summarised in a MultiQC report [68]. Raw counts were then analysed with Degust [69], a web tool that performs normalisation using trimmed mean of M-values (TMM) [70], and differential expression analysis performed using *limma* [71] and *voom* [72]. AGG *mdx* model was expressed relative to WT exercised control to rule out the effects of exercise-related adaptations. The data presented in heatmaps was considered statistically significantly different based on a threshold of a \log^{-2} fold-change ($\log_2\text{FC}$) of $\pm > 1.0$ (2-fold difference with a corresponding FDR of < 0.05).

4.13. Western blotting

We used western blotting to measure DMFs capacity to engage and activate the expression of the Nrf2/Kelch-like ECH-associated protein 1 (Keap1) pathway and downstream cytoprotective antioxidant proteins. Briefly, primary antibodies: anti-phospho-NF-κB p65 (Ser536) (1:750; 3033; CST), anti-NF-κB p65 (1:1000; 8242; CST), anti-Nrf2 (1:1000, 12721; CST), anti-Keap1 (1:1000; 8047; CST), anti-NAD(P)H dehydrogenase:quinone oxidoreductase (NQO1) (1:1000; 62262; CST) and anti-superoxide dismutase 1 (SOD1) (1:1000; ADI-SOD-101; Enzo Life Sciences) were used. Membranes were probed with a horseradish peroxidase (HRP)-conjugated secondary antibody (all 1:5000; anti-rabbit IgG, Vector Laboratories) in 5 % non-fat milk powder in for 1 h at room temperature followed by imaging, Coomassie blue staining and normalisation to total protein. For further details on the method used, see our previous work [12,73].

4.14. Statistics

Data are presented as mean \pm standard error of the mean (SEM) unless otherwise stated. One-way ANOVAs were performed using Prism software (GraphPad, La Jolla, CA) for all analyses unless otherwise stated to assess either the extent of phenotype or *mdx* VEH relative to treatment groups and Tukey's post hoc test was used for multiple comparisons. For contractile force-frequency experiments, a two-way ANOVA with repeated measures was performed using Sidak post hoc testing to interrogate differences between phenotype/treatment and time/frequency. A $P < 0.05$ was considered significant and trends were reported at $P < 0.1$. Outliers were removed if outside ± 2 standard deviations from the mean.

CRedit authorship contribution statement

Stephanie Kourakis: Writing – review & editing, Writing – original draft, Project administration, Methodology, Investigation, Formal analysis, Data curation. **Cara A. Timpani:** Writing – review & editing, Writing – original draft, Supervision, Project administration, Methodology, Funding acquisition, Formal analysis, Data curation, Conceptualization. **Ryan M. Bagaric:** Writing – review & editing, Methodology. **Bo Qi:** Writing – review & editing, Methodology. **Rebecca Boyer:** Writing – review & editing, Methodology. **Guinevere Spiesberger:** Writing – review & editing, Methodology. **Nitika Kandhari:** Writing – review & editing, Formal analysis, Data curation. **Xu Yan:** Writing – review &

editing, Methodology. **Jujiao Kuang:** Writing – review & editing, Methodology. **Ankita Tulangekar:** Data curation, Writing – review & editing. **Judy B. de Haan:** Writing – review & editing. **Deanna Deveson-Lucas:** Writing – review & editing, Formal analysis, Data curation. **Nicole Stupka:** Writing – review & editing, Methodology. **Dirk Fischer:** Writing – review & editing, Conceptualization. **Emma Rybalka:** Writing – review & editing, Writing – original draft, Supervision, Resources, Project administration, Methodology, Investigation, Funding acquisition, Formal analysis, Data curation, Conceptualization.

Declaration of competing interest

The authors declare the following financial interests/personal relationships which may be considered as potential competing interests: Emma Rybalka reports financial support was provided by The Muscular Dystrophy Association U.S.A. ER's lab is supported by AFM Téléthon (France), The Jack Brockhoff Foundation and Duchenne Parent Project Netherlands. ER discloses consultancy work for Santhera Pharmaceuticals, Epirium Bio and Cure ADSSL1 outside of this project. If there are other authors, they declare that they have no known competing financial interests or personal relationships that could have appeared to influence the work reported in this paper.

Acknowledgments

This work was supported by funding from The Muscular Dystrophy Association U.S.A (Ideas grant: MDA871929). ER's lab is supported by AFM Téléthon (France), The Jack Brockhoff Foundation (Australia) and Duchenne Parent Project Netherlands. SK, CAT, and ER acknowledge outstanding support from Anne Luxford, Tricia Murphy, and Steve Holloway with animal care and breeding; Valentina Jovanovska for technical support; Thomas Yates for assistance with heatmap generation; The Melbourne Histology Platform, The University of Melbourne, for tissue embedding, sectioning, and staining support; and Annemieke Aartsma-Rus and Maaiké Van Putten, Leiden University Medical Centre, for advice on the exercise aggravation protocol and critical reading of the manuscript. Schematics were created with BioRender.com and figures were constructed in Adobe Illustrator.

Appendix A. Supplementary data

Supplementary data to this article can be found online at <https://doi.org/10.1016/j.redox.2025.103676>.

Data availability

Data will be made available on request.

References

- [1] D. Duan, N. Goemans, S.i. Takeda, E. Mercuri, A. Aartsma-Rus, Duchenne muscular dystrophy, *Nat. Rev. Dis. Primers* 7 (2021) 13.
- [2] L. Wahlgren, A.-K. Kroksmark, A. Lindblad, M. Tulinius, K. Sofou, Respiratory comorbidities and treatments in Duchenne muscular dystrophy: impact on life expectancy and causes of death, *J. Neurol.* (2024), <https://doi.org/10.1007/s00415-024-12372-7>.
- [3] L. Passamano, et al., Improvement of survival in Duchenne Muscular Dystrophy: retrospective analysis of 835 patients, *Acta Myol.* 31 (2012) 121–125.
- [4] J.E. Archer, A.C. Gardner, H.P. Roper, A.A. Chikermane, A.J. Tatman, Duchenne muscular dystrophy: the management of scoliosis, *J. Spine Surg.* 2 (2016) 185–194.
- [5] S. Szwec, Z. Kaplucha, J.S. Chamberlain, P. Konieczny, Dystrophin- and utrophin-based therapeutic approaches for treatment of duchenne muscular dystrophy: a comparative review, *BioDrugs* 38 (2024) 95–119.
- [6] A. Lek, et al., Death after high-dose rAAV9 gene therapy in a patient with duchenne's muscular dystrophy, *N. Engl. J. Med.* 389 (2023) 1203–1210.
- [7] A. Tulangekar, T.E. Sztal, Inflammation in duchenne muscular dystrophy-exploring the role of neutrophils in muscle damage and regeneration, *Biomedicines* 9 (2021).
- [8] S. Kourakis, et al., Standard of care versus new-wave corticosteroids in the treatment of Duchenne muscular dystrophy: can we do better? *Orphanet J. Rare Dis.* 16 (2021) 117.
- [9] L. Cowen, M. Mancini, A. Martin, A. Lucas, J.M. Donovan, Variability and trends in corticosteroid use by male United States participants with Duchenne muscular dystrophy in the Duchenne Registry, *BMC Neurol.* 19 (2019) 84.
- [10] J.K. Mah, et al., Efficacy and safety of vamorolone in duchenne muscular dystrophy: a 30-month nonrandomized controlled open-label extension trial, *JAMA Netw. Open* 5 (2022) e2144178.
- [11] S. Kourakis, et al., Targeting Nrf2 for the treatment of duchenne muscular dystrophy, *Redox Biol.* 38 (2021) 101803.
- [12] C.A. Timpani, et al., Dimethyl fumarate modulates the dystrophic disease program following short-term treatment, *JCI Insight* (2023), <https://doi.org/10.1172/jci.insight.165974>.
- [13] R. Willmann, et al., Enhancing translation: guidelines for standard pre-clinical experiments in mdx mice, *Neuromuscul. Disord.* 22 (2012) 43–49.
- [14] A. De Luca, Use of treadmill and wheel exercise for impact on mdx mice phenotype (SOP DMD_M.2.1.001). https://www.treat-nmd.org/wp-content/uploads/2023/07/MDX-DMD_M.2.1.001.pdf.
- [15] K.E. Schill, et al., Muscle damage, metabolism, and oxidative stress in mdx mice: impact of aerobic running, *Muscle Nerve* 54 (2016) 110–117.
- [16] L.M. Ward, D.R. Weber, Growth, pubertal development, and skeletal health in boys with Duchenne Muscular Dystrophy, *Curr. Opin. Endocrinol. Diabetes Obes.* 26 (2019) 39–48.
- [17] X. Suárez-Calvet, et al., Decoding the transcriptome of Duchenne muscular dystrophy to the single nuclei level reveals clinical-genetic correlations, *Cell Death Dis.* 14 (2023) 596.
- [18] P.M. Clarkson, et al., ACTN3 genotype is associated with increases in muscle strength in response to resistance training in women, *J. Appl. Physiol.* 99 (2005) 154–163.
- [19] C.T. Pappas, P.A. Krieg, C.C. Gregorio, Nebulin regulates actin filament lengths by a stabilization mechanism, *Journal of Cell Biology* 189 (2010) 859–870.
- [20] M. Ogundele, et al., Validation of chemokine biomarkers in duchenne muscular dystrophy, *Life (Basel)* 11 (2021).
- [21] A. R. S. Mohan, C. Vellapandian, A voyage on the role of nuclear factor kappa B (NF- κ B) signaling pathway in duchenne muscular dystrophy: an inherited muscle disorder, *Cureus* 16 (2024) e67901.
- [22] J.D. Porter, et al., Persistent over-expression of specific CC class chemokines correlates with macrophage and T-cell recruitment in mdx skeletal muscle, *Neuromuscul. Disord.* 13 (2003) 223–235.
- [23] J. Morroni, et al., Accelerating the mdx heart histo-pathology through physical exercise, *Life* 11 (2021) 706.
- [24] S.D. Lombardo, et al., A network medicine approach for drug repurposing in duchenne muscular dystrophy, *Genes (Basel)* 12 (2021).
- [25] S. Hanna, et al., Late-stage skeletal muscle transcriptome in duchenne muscular dystrophy shows a BMP4-induced molecular signature, *bioRxiv* (2024), <https://doi.org/10.1101/2024.04.19.590266>, 2024.2004.2019.590266.
- [26] S. Vianello, et al., SPP1 genotype and glucocorticoid treatment modify osteopontin expression in Duchenne muscular dystrophy cells, *Hum. Mol. Genet.* 26 (2017) 3342–3351.
- [27] Z.M. Howard, et al., Mineralocorticoid receptor antagonists and glucocorticoids differentially affect skeletal muscle inflammation and pathology in muscular dystrophy, *JCI Insight* 7 (2022).
- [28] N. Ramshanker, et al., Effects of prednisolone on serum and tissue fluid IGF-I receptor activation and post-receptor signaling in humans, *J. Clin. Endocrinol. Metabol.* 102 (2017) 4031–4040.
- [29] N.L. McRae, et al., Genetic reduction of the extracellular matrix protein versican attenuates inflammatory cell infiltration and improves contractile function in dystrophic mdx diaphragm muscles, *Sci. Rep.* 10 (2020) 11080.
- [30] Y. Hathout, et al., Disease-specific and glucocorticoid-responsive serum biomarkers for duchenne muscular dystrophy, *Sci. Rep.* 9 (2019) 12167.
- [31] J.S. Moylan, et al., Neutral sphingomyelinase-3 mediates TNF-stimulated oxidant activity in skeletal muscle, *Redox Biol.* 2 (2014) 910–920.
- [32] P. Bhargava, et al., Dimethyl fumarate treatment induces lipid metabolism alterations that are linked to immunological changes, *Ann. Clin. Transl. Neurol.* 6 (2019) 33–45.
- [33] Y. Hirotsu, et al., Nrf2-MafG heterodimers contribute globally to antioxidant and metabolic networks, *Nucleic Acids Res.* 40 (2012) 10228–10239.
- [34] T. Oyake, et al., Bach proteins belong to a novel family of BTB-basic leucine zipper transcription factors that interact with MafK and regulate transcription through the NF-E2 site, *Mol. Cell Biol.* 16 (1996) 6083–6095.
- [35] S. Liu, J. Pi, Q. Zhang, Signal amplification in the KEAP1-NRF2-ARE antioxidant response pathway, *Redox Biol.* 54 (2022) 102389.
- [36] X.J. Wang, J.D. Hayes, C.J. Henderson, C.R. Wolf, Identification of retinoic acid as an inhibitor of transcription factor Nrf2 through activation of retinoic acid receptor alpha, *Proc. Natl. Acad. Sci. U. S. A.* 104 (2007) 19589–19594.
- [37] M. Culbreth, M. Aschner, GSK-3 β , a double-edged sword in Nrf2 regulation: implications for neurological dysfunction and disease, *F1000Res* 7 (2018) 1043.
- [38] Y. Nakae, et al., Quantitative evaluation of the beneficial effects in the mdx mouse of epigallocatechin gallate, an antioxidant polyphenol from green tea, *Histochem. Cell Biol.* 137 (2012) 811–827.
- [39] P.F. Fiore, et al., Lack of PKC θ promotes regenerative ability of muscle stem cells in chronic muscle injury, *Int. J. Mol. Sci.* 21 (2020).
- [40] M.C. Hughes, et al., Impairments in left ventricular mitochondrial bioenergetics precede overt cardiac dysfunction and remodelling in Duchenne muscular dystrophy, *J. Physiol.* 598 (2020) 1377–1392.
- [41] J. Morroni, et al., Inhibition of PKC θ improves dystrophic heart phenotype and function in a novel model of DMD cardiomyopathy, *Int. J. Mol. Sci.* 23 (2022) 2256.

- [42] K. Kato, et al., Lung-targeted delivery of dimethyl fumarate promotes the reversal of age-dependent established lung fibrosis, *Antioxidants (Basel)* 11 (2022).
- [43] C.J. Oh, et al., Dimethylfumarate attenuates renal fibrosis via NF-E2-Related factor 2-mediated inhibition of transforming growth factor- β /smad signaling, *PLoS One* 7 (2012) e45870.
- [44] P.P. Laurila, et al., Inhibition of sphingolipid de novo synthesis counteracts muscular dystrophy, *Sci. Adv.* 8 (2022) eabh4423.
- [45] H.G. Radley-Crabb, et al., Dystropathology increases energy expenditure and protein turnover in the mdx mouse model of duchenne muscular dystrophy, *PLoS One* 9 (2014) e89277.
- [46] C. Mao, et al., Orthosteric and allosteric modulation of human HCAR2 signaling complex, *Nat. Commun.* 14 (2023) 7620.
- [47] T. Molina, P. Fabre, N.A. Dumont, Fibro-adipogenic progenitors in skeletal muscle homeostasis, regeneration and diseases, *Open Biol* 11 (2021) 210110.
- [48] E.R. Miranda, K. Funai, Suppression of de novo sphingolipid biosynthesis mitigates sarcopenia, *Nat Aging* 2 (2022) 1088–1089.
- [49] S. Dasgupta, S.K. Ray, Insights into abnormal sphingolipid metabolism in multiple sclerosis: targeting ceramide biosynthesis as a unique therapeutic strategy, *Ther. Targets. Neurol. Dis.* 4 (2017).
- [50] A.S. De la Garza-Rodea, et al., Sphingosine phosphate lyase is upregulated in duchenne muscular dystrophy, and its inhibition early in life attenuates inflammation and dystrophy in mdx mice, *Int. J. Mol. Sci.* 23 (2022).
- [51] R.B. Khattri, et al., Magnetic resonance quantification of skeletal muscle lipid infiltration in a humanized mouse model of Duchenne muscular dystrophy, *NMR Biomed.* 36 (2023) e4869.
- [52] S.L.S. Houwen-van Opstal, et al., BMI-z scores of boys with Duchenne muscular dystrophy already begin to increase before losing ambulation: a longitudinal exploration of BMI, corticosteroids and caloric intake, *Neuromuscul. Disord.* 32 (2022) 236–244.
- [53] P.J. Muire, L.H. Mangum, J.C. Wenke, Time course of immune response and immunomodulation during normal and delayed healing of musculoskeletal wounds, *Front. Immunol.* 11 (2020) 1056.
- [54] Y. Mao-Draayer, et al., Real-world safety and effectiveness of dimethyl fumarate in patients with MS: results from the ESTEEM Phase 4 and PROCLAIM Phase 3 studies with a focus on older patients, *Adv. Ther.* 42 (2025) 395–412.
- [55] K.S. Pandey, et al., Long-term safety and effectiveness of dimethyl fumarate in patients with multiple sclerosis treated in routine medical practice: final analysis of the ESTEEM study, *Neurology and Therapy* 14 (2025) 243–260.
- [56] S. Vucic, et al., Safety and efficacy of dimethyl fumarate in ALS: randomised controlled study, *Ann. Clin. Transl. Neurol.* 8 (2021) 1991–1999.
- [57] S. Kourakis, et al., Dimethyl fumarate and its esters: a drug with broad clinical utility? *Pharmaceuticals (Basel)* 13 (2020).
- [58] R.D. Mância, et al., Dystrophic phenotype improvement in the diaphragm muscle of mdx mice by diacerein, *PLoS One* 12 (2017) e0182449.
- [59] D.G. Campelj, et al., Sodium nitrate co-supplementation does not exacerbate low dose metronomic doxorubicin-induced cachexia in healthy mice, *Sci. Rep.* 10 (2020) 15044.
- [60] N. Laws, A. Hoey, Progression of kyphosis in mdx mice, *J. Appl. Physiol.* 97 (2004) 1970–1977, 1985.
- [61] C.A. Timpani, et al., Adenylosuccinic acid therapy ameliorates murine Duchenne Muscular Dystrophy, *Sci. Rep.* 10 (2020) 1125.
- [62] M. Grounds, **Quantification of histopathology in Haematoxylin and Eosin stained muscle sections (SOP DMD M.1.2.007)**. https://www.treat-nmd.org/wp-content/uploads/2023/07/MDX-DMD_M.1.2.007-28.pdf.
- [63] N. Stupka, et al., Activated calcineurin ameliorates contraction-induced injury to skeletal muscles of mdx dystrophic mice, *J. Physiol.* 575 (2006) 645–656.
- [64] W. Lin, et al., The effect of sleep restriction, with or without exercise, on skeletal muscle transcriptomic profiles in healthy young males, *Front Endocrinol (Lausanne)* 13 (2022) 863224.
- [65] P.E. Harshil Patel, Alexander Peltzer, Rickard Hammarén, Olga Botvinnik, Gregor Sturm, Denis Moreno, Pranathi Vemuri, Lorena Pantano silviamorins, Maxime U. Garcia FriederikeHanssen, Chris Cheshire, R. Fenouil, , nf-core bot, marchoeppner, Peng Zhou, Gisela Gabernet, Daniel Straub, Hörtenhuber Matthias, Nf-Core/Rnaseq: Nf-Core/rnaseq v3.2 - Copper Flamingo, 3.2, Zenodo, 2021.
- [66] A. Dobin, et al., STAR: ultrafast universal RNA-seq aligner, *Bioinformatics* 29 (2012) 15–21.
- [67] R. Patro, G. Duggal, M.I. Love, R.A. Irizarry, C. Kingsford, Salmon provides fast and bias-aware quantification of transcript expression, *Nat. Methods* 14 (2017) 417–419.
- [68] P. Ewels, M. Magnusson, S. Lundin, M. Käller, MultiQC: summarize analysis results for multiple tools and samples in a single report, *Bioinformatics* 32 (2016) 3047–3048.
- [69] A.P. David R. Powell, Michael Milton, Degust: Interactive Rna-Seq Analysis, 2019 (zenodo).
- [70] M.D. Robinson, A. Oshlack, A scaling normalization method for differential expression analysis of RNA-seq data, *Genome Biol.* 11 (2010) R25.
- [71] M.E. Ritchie, et al., Limma powers differential expression analyses for RNA-sequencing and microarray studies, *Nucleic Acids Res.* 43 (2015) e47, e47.
- [72] C.W. Law, Y. Chen, W. Shi, G.K. Smyth, voom: precision weights unlock linear model analysis tools for RNA-seq read counts, *Genome Biol.* 15 (2014) R29.
- [73] D.G. Campelj, et al., The paradoxical effect of PARP inhibitor BGP-15 on irinotecan-induced cachexia and skeletal muscle dysfunction, *Cancers (Basel)* 12 (2020).